STM/STS study on electronic superstructures in the superconducting state of high-T-c cuprate Bi2Sr2CaCu208+delta

STM/STS study on electronic superstructures in the superconducting state of high-T_c cuprate $Bi_2Sr_2CaCu_2O_{8+\delta}$

IOP Conf. Series: Journal of Physics: Conf. Series **969** (2018) 012071 doi:10.1088/1742-6596/969/1/012071

STM/STS study on electronic superstructures in the superconducting state of high-T_c cuprate $Bi_2Sr_2CaCu_2O_{8+\delta}$

S Mizuta[1], T Kurosawa[1], K Takeyama[2], N Momono[3], Y Ishii[1], H Yoshida[1], M Oda[1] and M Ido[1]

[1] Department of Physics, Hokkaido University, Sapporo 060-0810, Japan
[2] Department of Physics, Asahikawa Medical University, Asahikawa 078-8510, Japan
[3] Department of Applied Sciences, Muroran Institute of Technology, Muroran 050-8585, Japan

E-mail: moda@sci.hokudai.ac.jp

Abstract. We report STM/STS measurements at 8 K in underdoped $Bi_2Sr_2CaCu_2O_{8+\delta}$ crystals ($T_c = 76$ K and hole-doping level $p \sim 0.12$) whose energy spectra around the Fermi level are characterized by a two-gap structure consisting of spatially inhomogeneous pseudogap (PG) and comparatively homogeneous superconducting gap (SCG). Two electronic superstructures, checkerboard modulation (CBM) and Cu-O-Cu bond-centered modulation (BCM), are observed with mapping spectral weights at low energies within the SCG and the ratio of spectral weights at $\pm\Delta_{PG}$ (PG energy), respectively. On the basis of the present findings, we suggest that the lower-energy scale CBM is an intrinsic property of Cu-O planes and can coexist with the BCM whose characteristic energy is $\sim\Delta_{PG}$ in identical regions in real space.

1. Introduction

In high-T_c cuprates, it has been demonstrated by many spectroscopic techniques such as ARPES and STM/STS that the electronic states around the Fermi level exhibit distinct features in different momentum and/or energy regions [1–3]. The Fermi surface (FS) is roughly divided into two parts which are located around the nodal and antinodal points of a gap with $d_{x^2-y^2}$ symmetry, respectively (fig. 1(h)). In the antinodal region, consisting of incoherent electronic states, a pseudogap (PG) develops below around temperature T^* higher than T_c, and another energy gap, which has been considered to be due to pairing, also develops successively below around temperature T_{pair} [4, 5]. It has been revealed in STM/STS experiments on high-T_c cuprates $Bi_2Sr_2CaCu_2O_{8+\delta}$ (Bi2212), $Ca_{2-x}Na_xCuO_2Cl_2$ (Na-CCOC) and so on that the antinodal PG is very sensitive to disorders and tends to be spatially inhomogeneous in nanometer scale, although the pairing gap, whose amplitude is hereafter referred to as Δ_0, is comparatively homogeneous [3]. In particular, the PG inhomogeneity becomes marked in the underdoped (UD) region, in which the energy size Δ_{PG} seems to vary over a wide range from $\sim\Delta_0$ to a several times larger energy [3]. On the other hand, the nodal region, the so-called "Fermi arc," consisting of coherent electronic states, plays a role in the occurrence of superconductivity; a homogeneous d-wave superconducting (SC) gap (SCG) is formed in this region, which has been confirmed with the observation of energy-dependent Bogoliubov quasiparticle (QP) interference (QPI) patterns by STM/STS [6]. The nodal SCG smoothly connects with the antinodal pairing

gap. In the SC state, therefore, a *d*-wave gap seems to be formed apparently over the entire FS, in addition to the inhomogeneous PG developing in the antinodal region (fig. 1(h)).

It has been reported in UD Bi2212 and Na-CCOC crystals that besides the QPI patterns, other two electronic superstructures can also be observed by STM/STS. One of them is two-dimensional short-range checkerboard modulation (CBM) along the two Cu-O bond directions with a period of $4a\times4a$ (a: the lattice constant) [3, 7–12]. The other is Cu-O-Cu bond-centered modulation (BCM) with $4a$-wide unidirectional nano-domains which are oriented randomly along the two Cu-O bond directions [6, 13]. The characteristic energies of these electronic superstructures are of great interest for the understanding of their origins and relationship with the superconductivity and the PG phenomenon. Kohsaka *et al.* have demonstrated that BCM is observed by mapping the ratio of STS spectral weights at $\pm\Delta_{\rm PG}$, or the ratio of conductance peak heights [6], suggesting that the characteristic energy of BCM is of the order of the PG size. On the other hand, it has yet to reach a consensus on the energy region in which the CBM is observed. Furthermore, it remains unclear whether these two electronic superstructures coexist in identical regions in real space.

In the present study, we performed low-temperature (T = 8 K) STM/STS experiments in UD Bi2212 single crystals with $T_{\rm c}$ = 76 K and $p \sim 0.12$, and clarified the above mentioned problems for the electronic superstructures.

2. Experimental

In the present STM/STS experiments, we used two methods to obtain conductance (dI/dV) images corresponding to images of the local density of states (LDOS) at specified energies. The first one is the conventional method for STS, in which the bias voltage ($V_{\rm s}$) dependences of dI/dV, hereafter referred to as STS spectra, are first measured at many positions in an area and then, a dI/dV image is constructed with the mapping of dI/dV values at a specified $V_{\rm s}$ in the measured STS spectra. In this method, the tip height is set every measurement position so as to give a constant current (CC) under a high set-up bias voltage. Thus, dI/dV images in the conventional method are referred to as CC dI/dV images. On the other hand, dI/dV images in the other method are referred to as constant height (CH) dI/dV images for the following reason: In this method, the bias voltage is modulated with a small amplitude while taking a current image in CH mode, and the output of a lock-in amplifier corresponding to dI/dV is directly imaged [14]. The dI/dV imaging in CH mode or the CH dI/dV imaging will be substantially free from the so-called "set-point effect," which has been pointed out to appear on CC dI/dV images obtained by the conventional method [13, 15].

3. Results and Discussion

Figure 1 shows results obtained with the conventional method in the UD Bi2212 crystal. STS spectra were measured at 128×128 points within a square region of $\sim$13×13 nm^2. A representative STS spectrum, shown in fig. 1(f), is consistent with a two-gap structure; it exhibits broad PG peaks at $|V_{\rm s}| \sim 65$ mV and a subgap peak or shoulder at $|V_{\rm s}| \sim 25$ mV. The subgap size $\Delta_{\rm SG}$, which is comparatively homogeneous, 25 $\sim$ 30 meV for the entire region examined, is smaller than the *d*-wave SCG amplitude or pairing gap size expected at the antinodal point $\Delta_0 \sim 40$ meV, which has been estimated in ARPES and STM/STS experiments [3, 16], but it is still close to Δ_0. Such a subgap structure in STS spectra can be explained in terms of the superconductivity, because if the density of states near the Fermi level is completely suppressed in the vicinity of the antinodal point with the marked development of PG and no pairing gap opens up there, leading to a reduction of the effective pairing gap size.

Two-dimensional short-range CBM along the two Cu-O bond directions is observed in the CC dI/dV image for $V_{\rm s}$ = 25 mV (fig. 1(a)). In the Fourier transform (FT) map, where q_x and q_y axes are taken to be oriented towards the Bragg spots and reciprocal lattice units for both

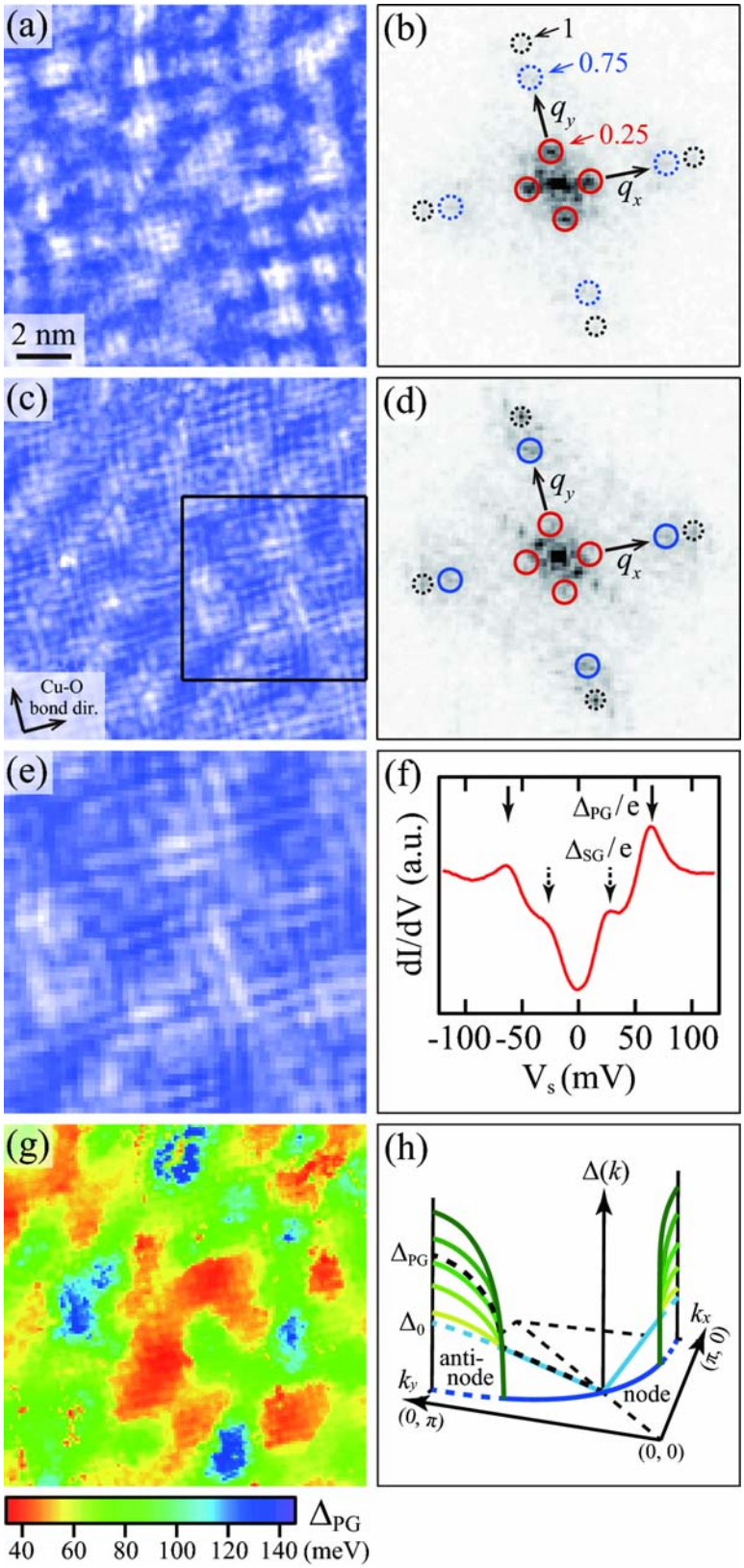

Figure 1. (a) CC dI/dV image for $V_s = 25$ mV and (b) the corresponding FT map. The black circles indicate the Bragg spots and, the red and blue ones denote Fourier spots at $|q| \sim 0.25$ and 0.75 on the q_x and q_y axes, respectively. (c) $Z(\boldsymbol{r}, e{=}1)$ map and (d) the corresponding FT map. (e) Magnified image of the boxed region in (c). (f) Representative example of STS spectra. (g) Map for PG size Δ_{PG}. (h) Schematic illustration of energy gaps on the Fermi surface at $T \ll T_c$. The black broken line represents the spatial average of partly inhomogeneous gap dispersions.

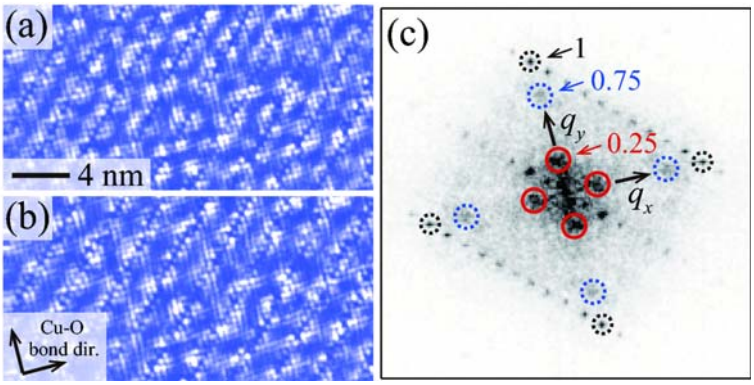

Figure 2. (a) CH dI/dV image for $V_s = 20$ mV and (b) for $V_s = -20$ mV. (c) FT map of the image for $V_s = 20$ mV. The black circles indicate the Bragg spots and, the red and blue ones denote Fourier spots at $|q| \sim 0.25$ and 0.75 in the q_x and q_y axes, respectively.

axes are defined as $2\pi/a = 1$, strong spots corresponding to the CBM are located at $|q| \sim 0.25$ on the q_x and q_y axes (fig. 1(b)), and their positions are independent of V_s (or energy); that is, the CBM is non-dispersive modulation. Thus, the period of CBM observed in the UD crystal is $\sim 4a \times 4a$. From analyses on the V_s dependence of the spot intensity at $|q| \sim 0.25$, it was also found that the CBM tends to be marked around an energy of $\sim\Delta_{SG}$, which is comparable to the effective pairing gap size. Furthermore, fainter spots are located at $|q| \sim 0.75$ on both axes in the FT map (fig. 1(b)). This result might suggest the existence of an internal structure in the CBM as reported in previous STM/STS studies [9]. In our experiments, however, the $|q| \sim 0.75$ components included in dI/dV images at $|V_s| \sim \Delta_{SG}/e$ were extremely weak, varying in their relative intensities with respect to the $|q| \sim 0.25$ ones (figs. 1(b) and 2(c)), and would be therefore extrinsic to the CBM. They could be rather explained in terms of the BCM whose characteristic energy is of the order of Δ_{PG}, taking into account the following feature of PG: The PG is not a complete gap but the so-called "soft gap" and therefore, the single QP spectra with central energies of $\sim\Delta_{PG}$, which are responsible for the BCM, would be very broad and have small but finite weights even at low energies around Δ_{SG}.

Previous STM/STS studies pointed out a possibility that the CBM in CC dI/dV images is affected by the set-point effect [13, 15]; at low energies below $\sim\Delta_0$, it may result from such an effect in the conventional method for STS. However, the CBM can be demonstrated by the CH dI/dV imaging which will be substantially free from the set-point effect. Figure 2 shows CH dI/dV images measured in an identical area for two bias voltages with opposite polarities, $V_s = \pm 20$ mV, and the corresponding FT map for $V_s = 20$ mV; the area is within the same cleaved surface as in the CC dI/dV image (fig. 1(a)). One can see in fig. 2 that CBM, which is characterized by very strong spots at $|q| \sim 0.25$ on the q_x and q_y axes in the FT map, is observed in CH dI/dV images for $|V_s| \sim \Delta_{SG}/e$. It should be noted here that the amplitude and phase of CBM in the real-space images (figs. 2(a) and (b)) are almost independent of bias polarity, although Neto *et al.* have reported that such an electronic superstructure is much more intense for positive sample bias voltages where STS spectra reflect electron-like QP states [17]. In fact, the CBM disappeared with mapping the ratio of dI/dV values at the two bias voltages with opposite polarities ($V_s = \pm 20$ mV). On the basis of our findings obtained by the CH dI/dV imaging, it is suggested that the CBM will be an intrinsic property of both electron- and hole-like QP states around $|E| \sim \Delta_{SG}$, at least in such UD Bi2212 crystals as the PG is strongly inhomogeneous in nanometer scale (see fig. 1(g)), which will be discussed in the next paragraph.

Shown in fig. 1(g) is a map of the PG size $\Delta_{\rm PG}$ determined from the peak position in STS spectra of the UD Bi2212 crystal (fig. 1(f)), which are the same with those used to construct the CC dI/dV image for $V_{\rm s} = 25$ mV (fig. 1(a)). In contrast to the subgap $\Delta_{\rm SG}$, the PG $\Delta_{\rm PG}$ is strongly inhomogeneous, varying over a wide energy range from ∼40 to ∼140 meV. Figure 1(c) is a map of the ratio of spectral weights at energies $E = \pm\Delta_{\rm PG}$, $Z(\boldsymbol{r},\ e \equiv E/\Delta_{\rm PG} = 1) \equiv \frac{dI}{dV}|_{+\Delta_{\rm PG}} / \frac{dI}{dV}|_{-\Delta_{\rm PG}}$, that is, a $Z(\boldsymbol{r},\ e = 1)$ map [6]. In this map, one can see unidirectional nonometer-scale domains, partially developing in some regions as in the boxed one, which is magnified two times in fig. 1(e) to make it more visible. As shown in the FT map (fig. 1(d)), comparatively strong spots are located at $|q| \sim 0.75$ on the q_x and q_y axes; furthermore, $|q| \sim 0.25$ spots can be confirmed although they are very weak. These features for the electronic superstructure observed around $\Delta_{\rm PG}$ are consistent with Cu-O-Cu bond-centered modulation (BCM), which consists of randomly oriented $4a$-wide nano-domains including an internal structure with a period of $4a/3$ [6, 13]. Interestingly, it is found from a comparison of the two images for $E \sim \Delta_{\rm SG}$ and $\Delta_{\rm PG}$ (figs. 1(a) and (c)) that the CBM is clearly observed in such regions as the BCM develops. This suggests that the two electronic superstructures with different characteristic energies can coexist in real space.

As is well known, the CBM is similar to one of the seven independent components in the QPI pattern, represented by wavevector $\boldsymbol{q}_1$. The $\boldsymbol{q}_1$ modulation, which has been demonstrated in STM/STS experiments on optimally doped Bi2212 under magnetic fields to be much more intense, together with the BCM, around vortex cores in the mixed state than in the pure SC state, has a weak dispersion at low bias voltages below $\sim\Delta_0/e$ and may have a phase depending on bias polarity [18]. On the other hand, the CBM, which develops markedly in the pure SC state, is non-dispersive and has a phase independent of bias polarity. Thus, the CBM seems to be distinct in some properties from the $\boldsymbol{q}_1$ modulation of QPI.

4. Summary

We performed STM/STS measurements at 8 K in UD Bi2212 crystals with $T_{\rm c} = 76$ K and $p \sim 0.12$ to examine the characteristic energy of CBM and its mutual relationship with the BCM whose characteristic energy is of the order of the spatially inhomogeneous PG. CBM, which has an energy-independent period of $\sim 4a \times 4a$, was observed at low energies around the subgap energy $\Delta_{\rm SG}$, comparable to the SCG size, not only by the conventional method (CC dI/dV imaging) but also by the CH dI/dV imaging that will be free from the set-point effect. This observation indicates that such a low-energy scale superstructure is an intrinsic property of Cu-O planes. Furthermore, it was demonstrated that the BCM is observed in some of the regions where the CBM appears clearly, suggesting that the two electronic superstructures with different characteristic energies can coexist in identical regions in real space.

Acknowledgments

We thank Professor Y. Toda for useful discussions. This work was partly supported by Grant-in-Aid for Scientific Research from the Ministry of Education, Culture, Sports, Science and Technology of Japan.

References

[1] Tanaka K *et al.* 2006 *Science* **314** 1910
[2] Kondo T *et al.* 2007 *Phys. Rev. Lett.* **98** 267004
[3] Kurosawa T *et al.* 2010 *Phys. Rev.* B **81** 094519
[4] Kondo T *et al.* 2011 *Nat. Phys.* **7** 21
[5] Kondo T *et al.* 2015 *Nat. Commun.* **6** 7699
[6] Kohsaka Y *et al.* 2008 *Nature* **454** 1072
[7] Howald C *et al.* 2003 *Phys. Rev.* B **67** 014533
[8] Vershinin M *et al.* 2004 *Science* **303** 1995

[9] Hanaguri T *et al.* 2004 *Nature* **430** 1001
[10] Momono N *et al.* 2005 *J. Phys. Soc. Jpn.* **74** 2400
[11] McElroy K *et al.* 2005 *Phys. Rev. Lett.* **94** 197005
[12] Liu Y H *et al.* 2007 *Phys. Rev.* B **75** 212507
[13] Kohsaka Y *et al.* 2007 *Science* **315** 1380
[14] Kurosawa T *et al.* 2016 *J. Phys. Soc. Jpn.* **85** 044709
[15] Hanaguri T *et al.* 2007 *Nat. Phys.* **3** 865
[16] Vishik I M *et al.* 2012 *Proc. Natl. Acad. Sci. USA* **109** 18332
[17] da Silva Neto E H *et al.* 2014 *Science* **343** 393
[18] Machida T, *et al.* 2016 *Nat. Commun.* **7** 11747